Pendulum as Vibration Absorber for Flexible Structures: Experiments and Theory

O. Cuvalci
Department of Mechanical Engineering,
Karadeniz Technical University,
Trabzon, Turkey

A. Ertas
Department of Mechanical Engineering,
Texas Tech University,
Lubbock, TX 79409

The dynamic response of a beam-tip mass-pendulum system subjected to a sinusoidal excitation is investigated. A simple pendulum mounted to a tip mass of a beam is used as a vibration absorber. The nonlinear equations of motion are developed to investigate the autoparametric interaction between the first two modes of the system. The nonlinear terms appear due to the curvature of the beam and the coupling effect between the beam and pendulum. Complete energy transfer between modes is shown to occur when the beam frequency is twice the pendulum frequency. Experimental results are compared with a theoretical solution obtained using numerical integration. The experimental results are in qualitative agreement with the theory.

1 Introduction

Many structures can be modeled as a continuous beam with concentrated mass at the end (Laura et al., 1974; Sato et al., 1978; Verma et al., 1978; Storch and Gates, 1985; Kojima et al., 1985; Gurgoze, 1986; Nagewara et al., 1986; Lui and Huang, 1988; and Zavodney and Nayfeh, 1989). Haxton and Barr (1972) studied a flexible column with tip-mass mounted on a large mass as a model for an autoparametric vibration absorber. Autoparametric vibration is a special case of parametric vibration said to exist when the conditions at internal resonance and external resonance are met simultaneously. The basic feature of autoparametric resonance is that the energy transfer (for example, in two degrees of freedom system) may occur when the lower mode frequency is equal to one-half the higher mode frequency. Due to the energy transfer, a lower mode may result in exponential response growth and may act as a vibration absorber to the excited mode (higher mode). Autoparametric resonance has been studied by numerous authors including Tondl (1963), Tomas (1967), Szemplinska-Stupnica (1969), Ibrahim (1975), Ibrahim and Barr (1978), Haddow and Barr (1984), Hatwall et al. (1983a, 1983b), and others.

In this study, a new model consisting of a flexible beam with a simple pendulum mounted on a tip mass as an autoparametric vibration absorber is presented (Fig. 1). There are many examples of vibration absorbers using the idea of mode interaction due to autoparametric resonance. Some of them were investigated by Crossley and Conn (1953), Arnold (1955), Eugene (1961), Struble and Heinbockel (1963), Masri and Caughey (1966), Masri (1972), Haxton and Barr (1972), Hatwal (1982), Hunt and Nissen (1982), Nissen et al. (1985), Shaw and Shaw, J and S. W. (1989), Ertas and Chew (1990), and B. Banerjee (1993).

For many years, resonance conditions and the problems associated with them have been among the most interesting and challenging phenomenon for engineers. In this study, the effectiveness of a passive dynamic vibration absorber within the autoparametric region has been investigated theoretically. A similar model was first studied by Ludeke (1942). He discussed the half-harmonic resonance occurrence rather than autoparametric resonance. In the present study, a series of parametric studies have been carried out to investigate the response of the nonlinear dynamics of the system for different tip mass-pendulum ratios and various pendulum damping coefficients when subjected to a sinusoidal excitation. Furthermore, experiments were performed to substantiate the energy transfer predicted theoretically.

This research will concentrate on the system dynamic response in the neighborhood of the internal resonance described by the following equation:

$$\omega_1 = 2\omega_2 \tag{1}$$

where ω_1, ω_2 and Ω are higher mode, lower mode, and forcing frequencies, respectively.

2 Mathematical Formulation

2.1 Derivation of Governing Equations. The model consists of a flexible beam rigidly clamped at the base with a simple pendulum mounted on a tip mass. It is assumed that the beam behaves like an Euler-Bernoulli beam. The clamped end of the beam has a harmonic base excitation of $y_g(t)$. Assuming that $\theta(\zeta, t)$ is the angular displacement of the beam as a function of location and time, the inextensibility condition can be written as

$$v'^2 + (1 + u')^2 = 1 \tag{2}$$

where $u(\zeta, t)$ and $v(\zeta, t)$ describes the displacements in the x and y directions, respectively, with respect to deformed axis at ζ and time t. Displacement, u with respect to displacement, v is given as

$$u(\zeta, t) = \zeta - \int_0^{\zeta} \sqrt{(1 - v'^2)}\, d\eta \tag{3}$$

where the prime symbol denotes differentiation with respect to s. The Euler-Bernoulli theory defines the bending moment of the beam and column as

$$M(s) = EI \frac{v''}{\sqrt{(1 - v'^2)}} \tag{4}$$

Referring to Fig. 1, the moments acting around the z-axis due to the forces at ζ can be written, respectively, as

Contributed by the Technical Committee on Vibration and Sound for publication in the JOURNAL OF VIBRATION AND ACOUSTICS. Manuscript received March 1994; revised March 1995. Associate Technical Editor: S. C. Sinha.

Copyright © 1996 by ASME
Downloaded From: https://vibrationacoustics.asmedigitalcollection.asme.org on 07/02/2019 Terms of Use: http://www.asme.org/about-asme/terms-of-use

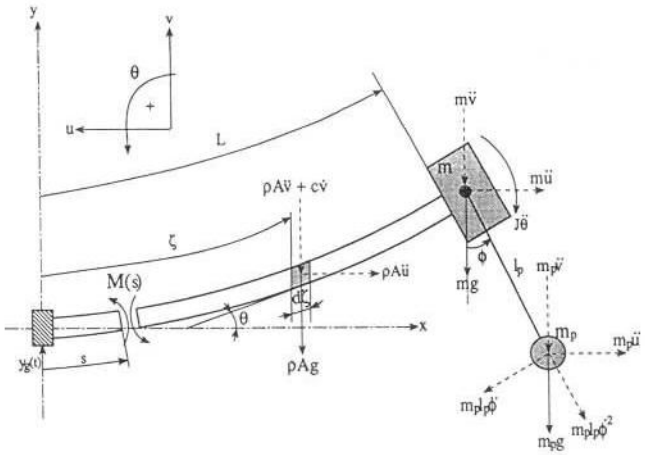

Fig. 1 Beam with a tip appendage

$$M_{u\zeta} = -\int_s^L \rho A\ddot{u}(\zeta, t)\int_s^\zeta \sin\theta(\eta, t)d\eta d\zeta \qquad (5)$$

and

$$M_{v\zeta} = -\int_s^L [\rho A\ddot{v}_t(\zeta, t) + c\dot{v}(\zeta, t)]\int_s^\zeta \cos\theta(\eta, t)d\eta d\zeta \quad (6)$$

where (.) represents the time derivative, ρA is the mass of the beam per unit length, and c is the damping of the beam. The first integral terms show the total internal forces acting on the beam, and the second integral terms show the moment arms in both of the above equations.

The moment equation is obtained in the x and y directions at $\zeta = L$ as

$$M_{uL} = [-(m + m_p)\ddot{u}(L, t) + m_p l_p[\ddot{\phi}\cos\phi(L, t) - \dot{\phi}^2\sin\phi(L, t)]\int_s^L \sin\phi(\zeta, t)d\zeta \quad (7)$$

and

$$M_{vL} = [-(m + m_p)\ddot{v}(L, t) - m_p l_p[\ddot{\phi}\sin\phi(L, t) + \dot{\phi}^2\cos\phi(L, t)]\int_s^L \cos\phi(\zeta, t)d\zeta \quad (8)$$

In Eqs. (7) and (8), m is the tip mass, m_p and l_p are the mass and length of the pendulum, and ϕ is the pendulum angular displacement being defined as positive in the counterclockwise direction. Differentiating Eqs. (4)–(8) twice with respect to s and equating the terms resulting from the bending moment to those from inertia and externally applied load yields the governing equation for the beam dynamics as

$$EI\left[\frac{v''''}{\sqrt{(1 - v'^2)}} + \frac{v''^3 + 3v'v''v'''}{\sqrt[3]{(1 - v'^2)}} + \frac{3v'^2v''^3}{\sqrt[5]{(1 - v'^2)}}\right] + \rho Av'\int_0^\zeta\left[\frac{\dot{v}'^2 + v'\ddot{v}'}{\sqrt{(1 - v'^2)}} + \frac{v'^2\dot{v}'^2}{\sqrt[3]{(1 - v'^2)}}\right]d\eta + \frac{v'v''}{\sqrt{(1 - v'^2)}}\left[\int_s^L (\rho A\ddot{v} + c\dot{v})d\zeta + \rho A\ddot{y}_g(L - s) + (m + m_p)(\ddot{v} + \ddot{y}_g) + m_p l_p(\ddot{\phi}\sin\phi + \dot{\phi}^2\cos\phi)\right] - v''\left\{\int_s^L \rho A\int_0^\zeta\left[\frac{\dot{v}'^2 + v'\ddot{v}'}{\sqrt{(1 - v'^2)}} + \frac{v'^2\dot{v}'^2}{\sqrt[3]{(1 - v'^2)}}\right]d\zeta d\eta + (m + m_p)\int_0^\zeta\left[\frac{\dot{v}'^2 + v'\ddot{v}'}{\sqrt{(1 - v'^2)}} + \frac{v'^2\dot{v}'^2}{\sqrt[3]{(1 - v'^2)}}\right]d\zeta - m_p l_p(\ddot{\phi}\sin\phi - \dot{\phi}^2\cos\phi)\right\} + \sqrt{(1 - v'^2)}[\rho A(\ddot{v} + \ddot{y}_g) + c\dot{v}] = 0 \quad (9)$$

Note that, since the pendulum damping, c_p, is very low, the effect of the $c_p\dot{\phi}$ term to the beam response was ignored in the above equation. The governing Eq. (9) includes higher order nonlinear terms. Expanding the slope-curvature terms by using the binomial expansion and eliminating terms of order higher than three yields

$$EI\left[v'''' + \tfrac{1}{2}v'^2v'''' + v''^3 + 3v'v''v'''\right] + \rho Av'\int_0^\zeta(\dot{v}'^2 + v'\ddot{v}')d\eta + v'v''\left[\int_s^L(\rho A\ddot{v} + c\dot{v})d\zeta + \rho A\ddot{y}_g(L - s) + (m + m_p)(\ddot{v} + \ddot{y}_g) + m_p l_p(\ddot{\phi}\sin\phi + \dot{\phi}^2\cos\phi)\right] - v''\left[\int_s^L \rho A\int_0^\zeta(\dot{v}'^2 + v'\ddot{v}')d\zeta d\eta + (m + m_p)\times\int_0^\zeta(\dot{v}'^2 + v'\ddot{v}')d\zeta - m_p l_p(\ddot{\phi}\cos\phi - \dot{\phi}^2\sin\phi)\right] + (1 - \tfrac{1}{2}v'^2)[\rho A(\ddot{v} + \ddot{y}_g) + c\dot{v}] = 0. \quad (10)$$

Nomenclature

c = damping coefficient of the beam
c_p = damping coefficient of the pendulum
E = modulus of elasticity
I = moment of inertia
J = polar moment of inertia
L = length of the beam
l_p = length of the pendulum
$M(s)$ = bending moment
m = tip mass
m_p = pendulum mass
ρA = mass of the beam per unit length
s = reference variable along the beam
t = time
u = axial deflection with respect to the deformed axis at ξ
v = transverse deflection with respect to the deformed axis at ξ
$\ddot{y}_g(t)$ = base acceleration
θ = angle of the deflection of the beam with x-axis
ϕ = pendulum angular displacement
w_b = circular frequency of the beam
w_p = circular frequency of the pendulum
Ω = forcing frequency
z_{max} = maximum steady state response of the beam
ϕ_{max} = maximum steady state response of the pendulum
ζ = deformed elastic axis of the beam
(′) = derivative with respect to s
(.) = derivative with respect to t

Downloaded From: https://vibrationacoustics.asmedigitalcollection.asme.org on 07/02/2019 Terms of Use: http://www.asme.org/about-asme/terms-of-use

Further, the equation of the pendulum can be obtained as

$$\ddot{\phi} + \frac{1}{l_p}(\ddot{v} + \ddot{y}_g + g)\sin\phi + \frac{\ddot{u}}{l_p}\cos\phi + \frac{c_p}{m_p l_p^2}(\dot{\theta} + \dot{\phi}) = 0. \quad (11)$$

where c_p is the damping coefficient at the pivot point of the pendulum and y_g is the base excitation. Taking the derivative of Eq. (3) with respect to time, expanding by using a binomial expansion, and eliminating terms of higher order than three yields

$$\ddot{u} = \int_0^\zeta (\dot{v}'^2 + v'\ddot{v}')d\zeta. \quad (12)$$

differentiating $\sin\theta = v'$ with respect to time and expanding by using a binomial expansion gives

$$\dot{\theta} = \dot{v}' + \tfrac{1}{2}v'^2\dot{v}', \quad (13)$$

where $\dot{\theta}$ is the angular velocity of the beam. Substituting Eqs. (12) and (13) into Eq. (11) yields

$$\ddot{\phi} + \frac{1}{l_p}(\ddot{v} + \ddot{y}_g + g)\sin\phi + \frac{1}{l_p}\int_0^\zeta (\dot{v}'^2 + v'\ddot{v}')d\zeta\cos\phi + \frac{c_p}{m_p l_p^2}\left(\dot{v}' + \frac{1}{2}v'^2\dot{v}' + \dot{\phi}\right) = 0 \quad (14)$$

The dynamics of the beam-tip mass-pendulum combination is defined by the nonlinear coupled Eqs. (10) and (14). Since the closed form solution cannot be obtained, Eqs. (10) and (14) should be transformed to the ordinary differential equation form by using one of the weighted residual methods. The Galerkin method is used as a transformation method in this study.

2.2 Truncated Equations. The response of the nonlinear problem can be defined as

$$v(s, t) = \sum_{i=1}^{n} r y_i(s) z_i(t) \quad (15)$$

where r is the scaling factor, $y_i(s)$ is the eigenfunction, which is the solution of the linear eigenvalue problem, and $z_i(t)$ is time dependent unknown time modulations of the corresponding eigenfunctions. In this study, in applying the Galerkin method the modal series will be truncated at the first mode, so that

$$v(s, t) = r y(s) z(t) \quad (16)$$

Substituting Eq. (16) into the partial differential Eq. (10) and orthogonalizing the error with respect to the eigenfunction yields the following ordinary differential equation

$$G_1\ddot{z} + G_2\ddot{z}z^2 + G_3c\dot{z} + G_4c\dot{z}z^2 + G_5\dot{z}^2z + (G_6 + t_{13}\ddot{\phi}\cos\phi + t_{14}\dot{\phi}^2\sin\phi)z + (G_7\ddot{y}_g + t_{17}\ddot{\phi}\sin\phi + t_{18}\dot{\phi}^2\cos\phi)z^2 + G_8z^3 + G_9\ddot{y}_g = 0, \quad (17)$$

where G and t are the coefficients obtained after applying the Galerkin method. Following the same procedure, the pendulum equation can be obtained as

$$\ddot{\phi} + \frac{1}{l_p}(P_4\ddot{z} + \ddot{y}_g + g)\sin\phi + \frac{P_1}{l_p}(\dot{z}^2 + z\ddot{z})\cos\phi + \frac{c_p}{m_p l_p^2}\left(P_2\dot{z} + \frac{1}{2}P_3\dot{z}z^2 + \dot{\phi}\right) = 0, \quad (18)$$

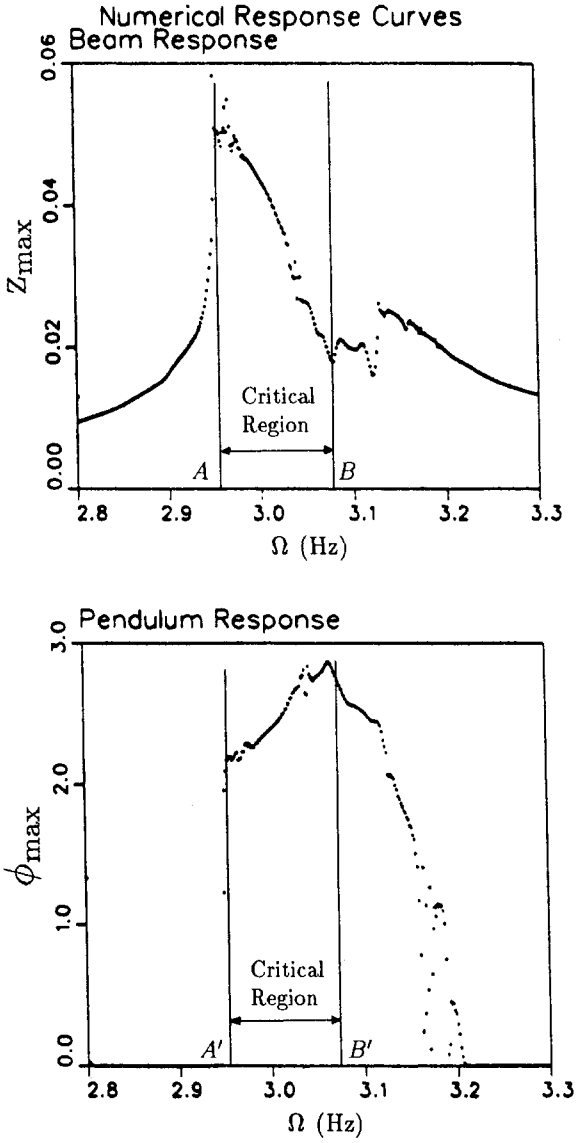

Fig. 2 Frequency response curves for f = 0.00025 m, $m_p/m \approx 1/4$, c_b = 0.10999 kg/s, c_p = 0.04364 kg/s, and EI = 1.373974 Nm²

where P_1, P_2, P_3, and P_4 are the coefficients obtained after applying the Galerkin method.

3 Numerical Results

The results of numerical integration are presented for the system parameters: A = 40.464 E-06 m², ρ = 7830 kg/m³, m = 0.212 kg, L = 0.336 m, I = 8.669867 E-12 m⁴. The parameters varied are c_p, and m/m_p. For all the numerical analyses, the internal frequency ratio of $\frac{1}{2}$, the time step dt = 0.01 seconds, and the frequency sweep by an increment of 0.0015 Hz are taken to be constant.

Figures 2, and 3 show the beam and pendulum response amplitudes as a function of forcing frequency, Ω, for the forcing frequency amplitude of 0.25 mm peak-to-peak, the natural frequency of the beam, ω_b = 3.07 Hz, the natural frequency of the pendulum, ω_p = 1.535 Hz, and $m/m_p = \frac{1}{4}$. These two figures reveal that the response of the beam and pendulum and the energy exchange between the modes are related to the pendulum damping coefficient. As the damping coefficient, c_p, decreases autoparametric interaction between the two modes becomes stronger. Figure 3 shows a strong autoparametric interaction between the beam and the pendulum when the excitation fre-

Downloaded From: https://vibrationacoustics.asmedigitalcollection.asme.org on 07/02/2019 Terms of Use: http://www.asme.org/about-asme/terms-of-use

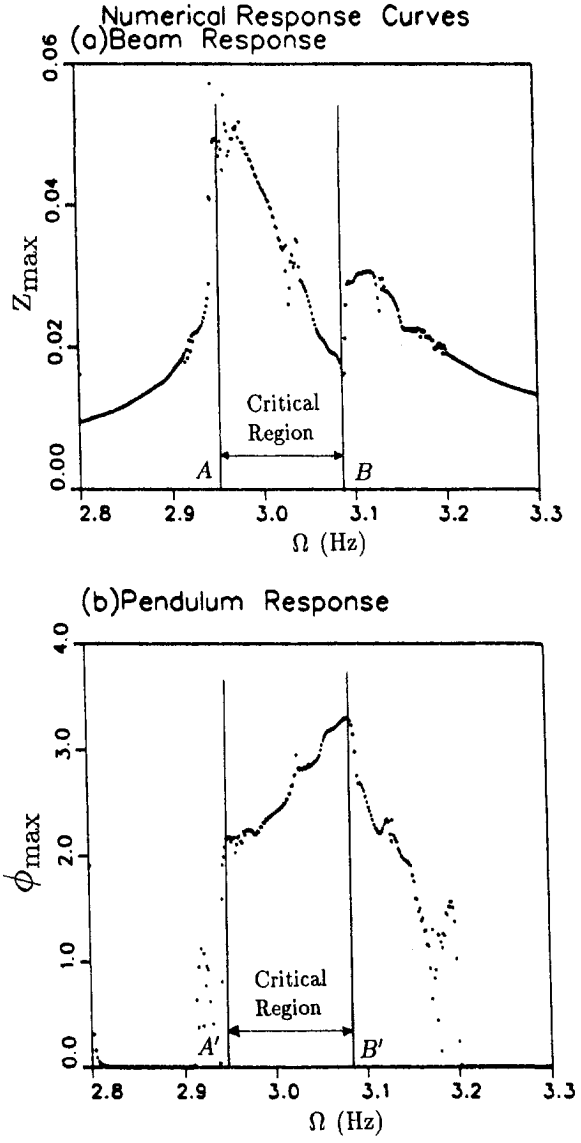

Fig. 3 Frequency response curves for f = 0.00025 m, $m_p/m \approx 1/4$, c_b = 0.10999 kg/s, c_p = 0.02182 kg/s, and EI = 1.373974 Nm^2

quency, Ω, reaches approximately 2.95 Hz and the first jump phenomenon is observed. At this point, namely point A, A', when the pendulum starts to oscillate, energy is being transferred to it. Points A and A' on the response curve are important as they define the starting point of the critical region (autoparametric region) of the energy exchange. The critical region ends at points B and B′, where the frequency of the beam response is $\Omega = \omega_b$ = 3.07 Hz. From this figure, it is evident that the amplitude of the beam is decreased and the energy is transferred to the pendulum when the primary resonance case is reached.

Figures 2 and 4 show the frequency response curves of the beam and the pendulum for different mass ratios. The mass ratios of the beam to the pendulum are chosen as $\frac{1}{5}$ and $\frac{1}{4}$, and corresponding frequencies of the beam with the tip mass become 3.14 and 3.07 Hz, respectively. Since the smaller pendulum has less inertia, comparison of Figs. 2 and 4 indicates that more energy is absorbed by the smaller pendulum. It is noteworthy to mention that the pendulum with smaller mass may have a response of more than one period and eventually experiences irregular motion even when the excitation amplitude is small. Figures 3 and 5 show that different values of forcing amplitude give the same trend for system response. However, comparison of these two figures reveals that the autoparametric interaction region changes with respect to the forcing amplitude. Higher forcing amplitude results in a larger range of frequency for absorption action.

4 Experimental Procedures and Equipment

The beam material and the length, the tip mass and the damping coefficient of the beam were taken to be constant (L = 336 mm, m = 212 gr, and c_b = 0.07 kg s/m) for all experiments. The experiment was conducted for two main parameters, namely the forcing amplitude and the pendulum mass. The experiments are performed in the frequency interval 2.0 to 3.8 Hz to obtain the frequency response curves. This interval covers the first natural frequency of the beam and integer multiples of the pendulum frequency.

The Macintosh 11fx80 was used as the computer including MIO-16 and NB-DMA boards and LabVIEW software. The LabVIEW software was used to program the MIO-16 board to record two-channel signals from the system as the beam and the pendulum response. The sampling rate, Δt, was assumed to be 0.02 sec. The experiments were performed in approximately 10 minutes for frequency response curves for the forcing

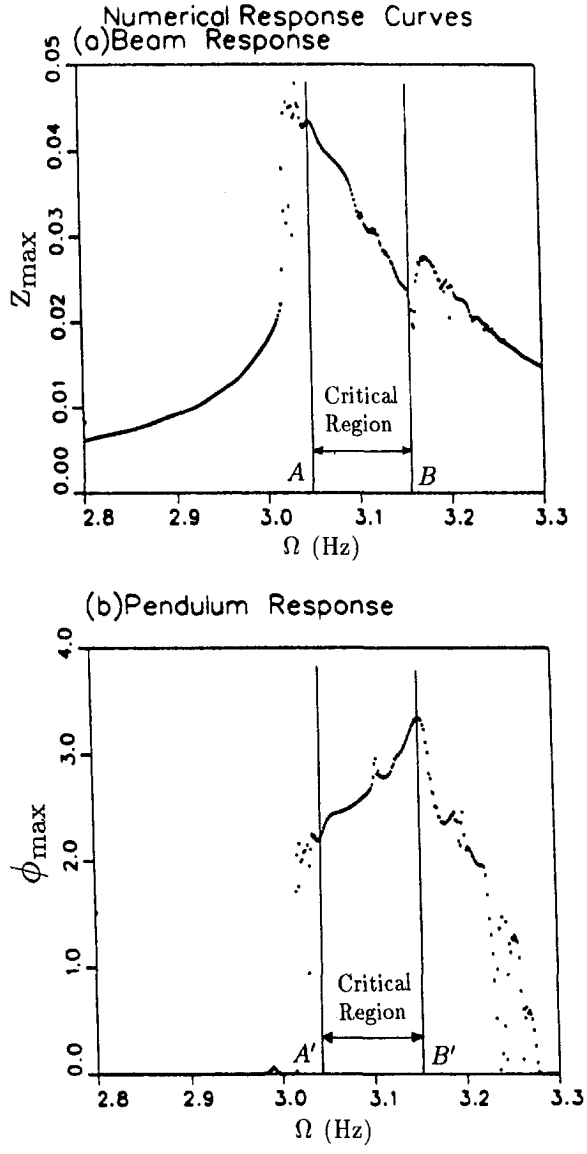

Fig. 4 Frequency response curves for f = 0.00025 m, $m_p/m \approx 1/5$, c_b = 0.10999 kg/s, c_p = 0.17455 kg/s, and EI = 1.373974 Nm^2

Downloaded From: https://vibrationacoustics.asmedigitalcollection.asme.org on 07/02/2019 Terms of Use: http://www.asme.org/about-asme/terms-of-use

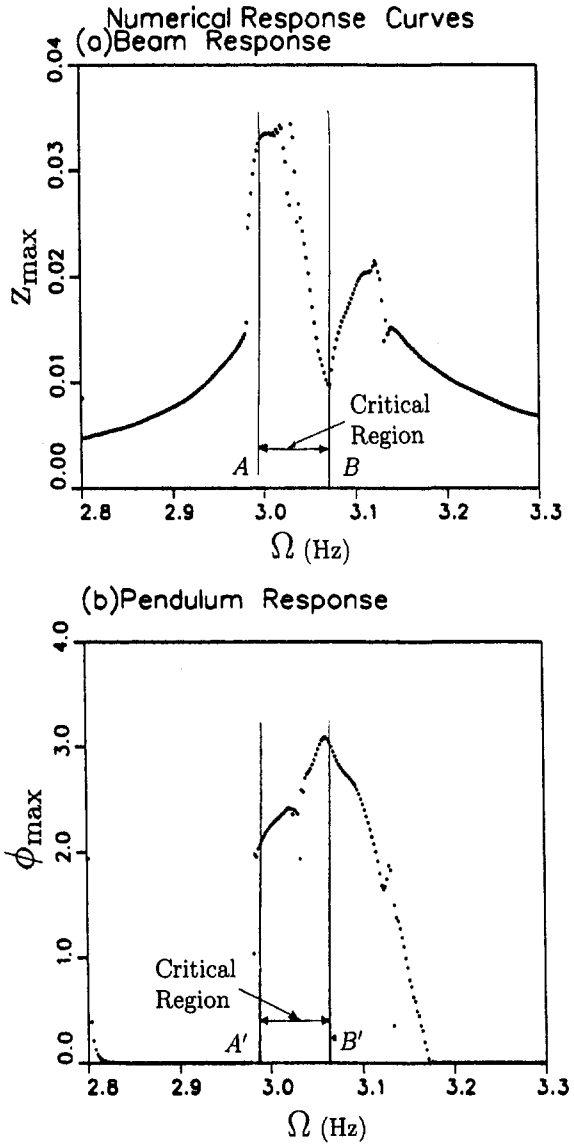

Fig. 5 Frequency response curves for f = 0.000125 m, $m_p/m \approx 1/4$, c_b = 0.10999 kg/s, c_p = 0.02182 kg/s, and EI = 1.373974 Nm^2

frequency interval 1.8 Hz, and in approximately 2 minutes for specified forcing frequencies. This experimental duration was considered to be long enough to observe all possible dynamics characteristics of the system and to eliminate the transient effects due to changes in excitation frequency. The experimental analysis was performed for four cases and the following diagrams are plotted to show the detail dynamics of the system:

(1) frequency response curve,
(2) time history,
(3) FFT, and
(4) phase plane.

The MB Dynamics Model C10E electrodynamic shaker was used as the vibrating equipment. It has 1,200 lbs force output rating and 1-inch peak-to-peak displacement. It is powered by an MB Dynamics solid-state Model S6K power amplifier. The excitation frequency range (lower and upper limits), frequency increment, and excitation amplitude were programmed by using the vibration control system. Excitation frequency was incrementally varied between these limits during the experiment, or, if desired, the frequency was held constant during the experiment. The Model 701LM Sweep Generator was used as the exciter for a vibration control system which provides the frequency range from 0.2 Hz to 5,000 Hz. The Model 801B Compressor was used to provide automatic level control in systems using frequencies from 2 to 10 kHz to provide automatic signal compression. The Model 801B Compressor can receive two feedback signals. Any two of the three signals, (namely, acceleration, velocity, and displacement) can be used to control the output from the sweep generator-compressor combination. The Model 610B Vibration Monitor was used separately as a standalone vibration monitor; also, it was used as part of the control system. The sweep generator and compressor were used to monitor and control the vibration system. The Model 831A Multi-Level Programmer was used for setting four different levels of excitation. An accelerometer was used for a feedback signal to control the shaker system. The Data 6000 is used to analyze the natural frequency, excitation signal condition, and the FFT of the response during the experiment.

The opto-digital device connected to the tip mass measures the relative rotation between the tip mass and pendulum from the vertical downward position. The opto-digital device has a linear response over a ∓ 180 degree range, therefore, the full-phase response of the pendulum can be obtained (Ertas and Mustafa, 1992). The opto-digital angle measurement system consists of four components: (1) optical encoder, (2) encoder/counter module, (3) analog-out module, and (4) programmable controller. These four components, along with an analog-in module, constitute a digitally programmable control system. The programmable controller forms the central element in the control system. It acquires and transmits information to and from various components. The control strategy is implemented via programs written in a special purpose language called the Ladder Logic. A Ladder Logic program is a list of instructions that the processor executes.

The opto-digital angle measurement system consists of an optical incremental shaft encoder (Disc Instruments, E20 series)

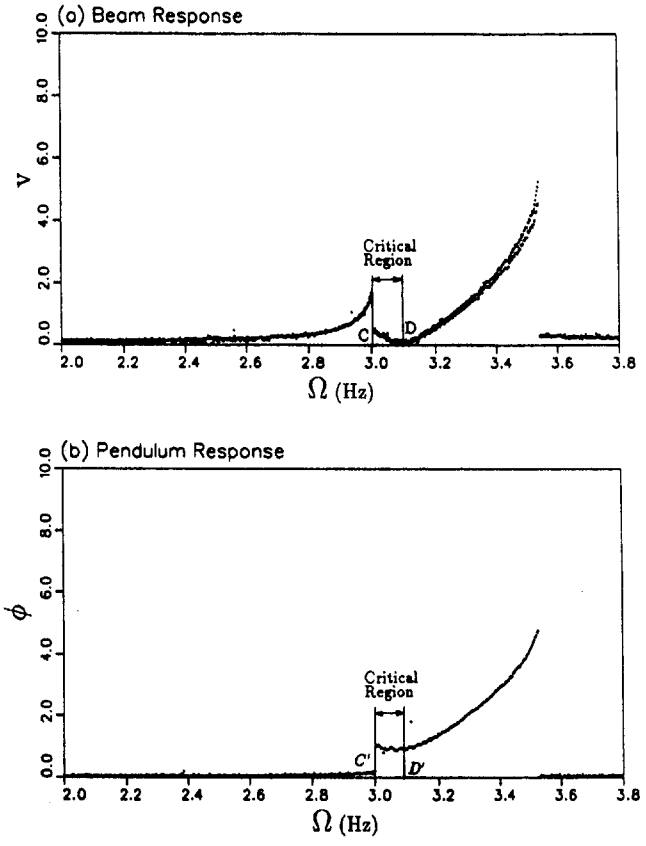

Fig. 6 Frequency response curves for f = 0.00025 m and $m_p/m \approx 1/4$

Downloaded From: https://vibrationacoustics.asmedigitalcollection.asme.org on 07/02/2019 Terms of Use: http://www.asme.org/about-asme/terms-of-use

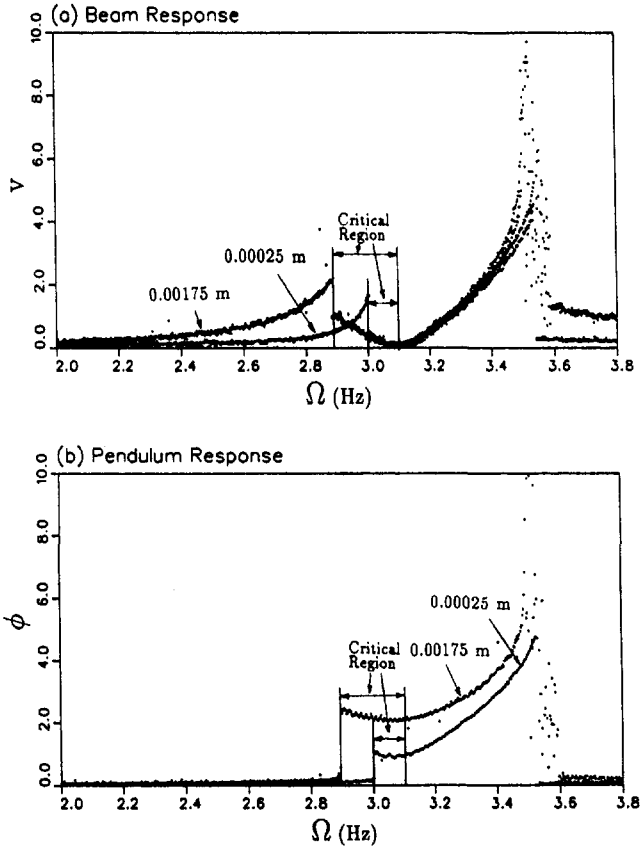

Fig. 7 Frequency response curves for f = 0.00025 m, f = 0.00175 m, and $m_p/m \approx 1/4$

that produces 4096 pulses per revolution of the shaft. The encoder has three outputs, channels A and B and an index. The outputs from channels A and B are square waves that are slightly out of phase. The encoder consists of a perforated disc, with a light source on one side and a photo sensor on the other. As the disc is rotated, the light passes through the perforations and is detected by the sensor, which produces an electrical pulse. The pulses are then counted by an optical encoder/counter module (Allen-Bradley 1771-IJ). The encoder module, by comparing the phase relationship between channels A and B, can detect a change in direction of rotation; hence, it can count up or down. This count is passed to the programmable controller (Allen-Bradley PLC 2/16) and then to an analog output module (Allen-Bradley 1771-OFE), where it is converted to an analog signal proportional to the count. The opto-digital angle measurement system described above provides a robust and reliable alternative to existing measurement techniques.

5 Experimental Results

For the first experiment, the mass ratio of the tip-mass of the beam, m and the pendulum mass, m_p was taken to be approximately $\frac{1}{4}$. The natural frequency of the beam then becomes ω_b = 3.07 Hz, and the natural frequency of the pendulum is set to ω_p = 1.535 Hz to maintain the condition of the autoparametric interaction. Figure 6 shows the variation of the response amplitudes as a function of forcing frequency, Ω, for the forcing amplitude of 0.25 mm peak-to-peak. The forcing amplitude kept approximately constant in the neighborhood of the autoparametric resonance for all the experiments.

As shown in this figure, the vertical axes represents the beam response, V, interms of voltage, generated by the piezo film which is proportional to strains developed in the beam and the ϕ represents the pendulum response interms of voltage generated by the opto-digital device. The experiment was conducted in the interval 2.0–3.8 Hz. It is seen from the figure that even though the system is excited by the natural frequency of the beam, the pendulum is also excited because of the coupling between the beam and the pendulum. This figure shows a strong autoparametric interaction between the beam and the pendulum when the excitation frequency, Ω, reaches approximately 3.0 Hz and the first jump phenomenon is observed. At this point, namely point C, C', energy is transferred to the pendulum from the beam; hence, the pendulum starts oscillating. As mentioned previously, points C and C' on the response curve are the starting point of the critical region (autoparametric region) of the energy exchange. The critical region ends at points D and D', where the frequency of the beam response is $\Omega = \omega_b$ = 3.10 Hz. From this figure, it is evident that the amplitude of the beam is almost diminished and the total energy is absorbed by the pendulum when the primary resonance case is reached. In other words, the complete energy transfer between modes oc-

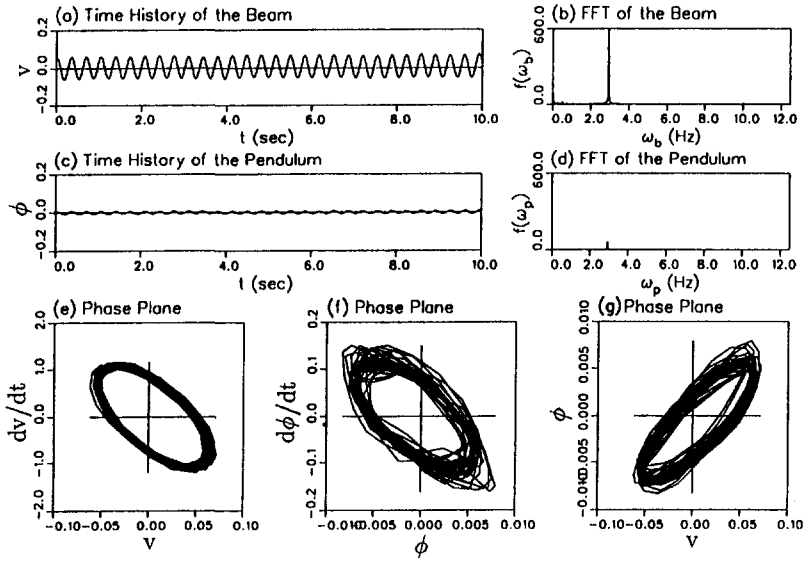

Fig. 8 Detail dynamics of the system for the forcing frequency of 2.95 Hz, f = 0.00025 m, and $m_p/m \approx 1/4$

Downloaded From: https://vibrationacoustics.asmedigitalcollection.asme.org on 07/02/2019 Terms of Use: http://www.asme.org/about-asme/terms-of-use

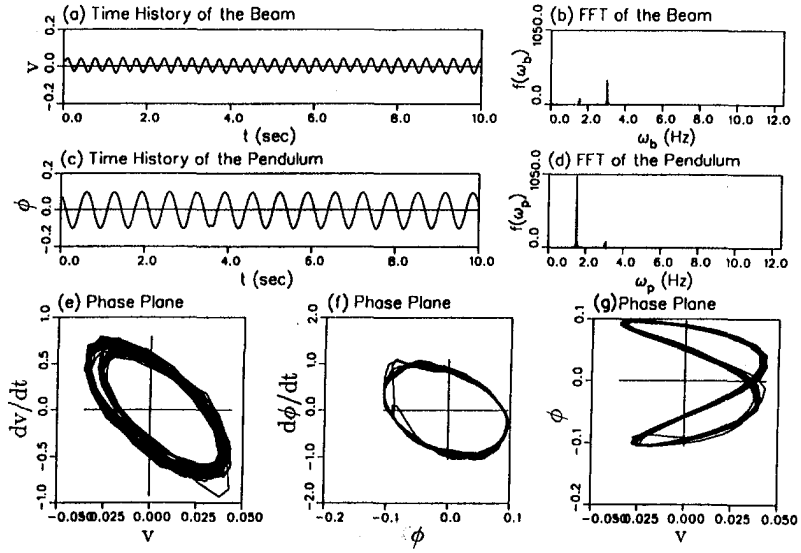

Fig. 9 Detail dynamics of the system for the forcing frequency of 3.02 Hz, f = 0.00025 m, and $m_p/m \approx 1/4$

curs when the beam frequency is twice the pendulum frequency and the forcing frequency is equal to beam frequency ($\omega_b = 2\omega_p$ and $\Omega = \omega_b$).

Figure 7 represents the change of the autoparametric interaction region with respect to forcing amplitude. As shown in this figure, when the structure is subjected to high forcing amplitude, absorption action will be within the larger range of frequency. When the structure is subjected to low forcing amplitude, absorption action will be within the small range of frequency. Figure 7 also reveals that the energy exchange from beam to pendulum is significantly increased when the system is under high amplitude excitation.

Figures 8(a) and 8(c) show the time history of the beam and the pendulum just before the first-jump phenomenon at Ω = 2.95 Hz. The FFT diagrams are shown in Figs. 8(b) and 8(d), respectively. Since the system is not within the autoparametric region at this point, the FFT diagrams show only excitation frequency, the pendulum and the beam are oscillating with Ω = 2.95 Hz because interaction between the beam and the pendulum has not yet begun. The noninteractive motion between the beam and the pendulum can also be verified by the projection of ϕ and $d\phi/dt$ plane (phase plane) as shown in Fig. 8(g). From this figure, it is clear that both the beam and the pendulum frequency ratios are one.

Figure 9 shows the complete dynamics of the beam and the pendulum at the frequency of 3.02 Hz within the critical region. With reference to Figures 9(b) and 9(d), it is seen that the pendulum frequency is one-half of the beam frequency. It is interesting to note that the second frequencies appear in the FFT plots as shown in Figs. 9(b) and 9(d). Namely, in Fig. 9(b), the dominant beam frequency is $\Omega = \omega_b$ = 3.02 Hz, and the the second frequency called the pendulum coupling frequency ω_p = 1.51 Hz. A similar coupling effect from the beam to the pendulum is also evident as shown in Fig. 9(d).

As shown in Fig. 10(a), when the natural frequency of the pendulum is tuned to cause internal resonance near the desired excitation frequency, beam response is minimized. It is anticipated that the maximum absorption action should occur when

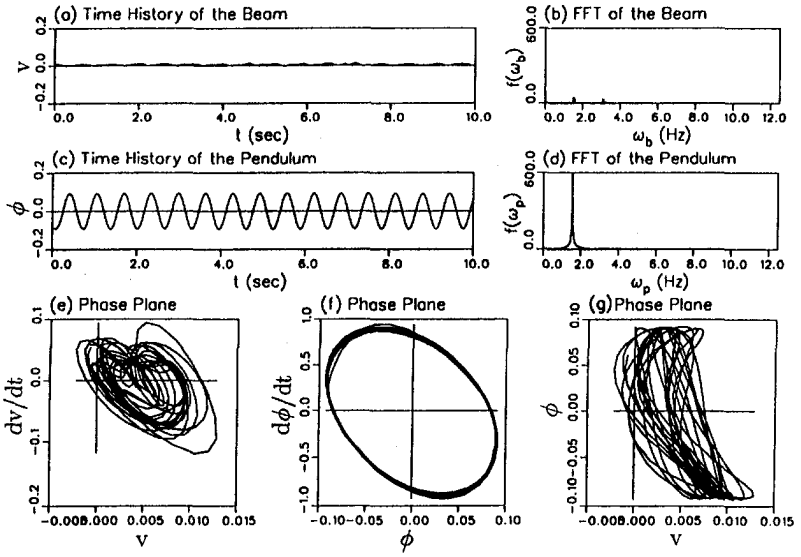

Fig. 10 Detail dynamics of the system for the forcing frequency of 3.10 Hz, f = 0.00025 m, and $m_p/m \approx 1/4$

Downloaded From: https://vibrationacoustics.asmedigitalcollection.asme.org on 07/02/2019 Terms of Use: http://www.asme.org/about-asme/terms-of-use

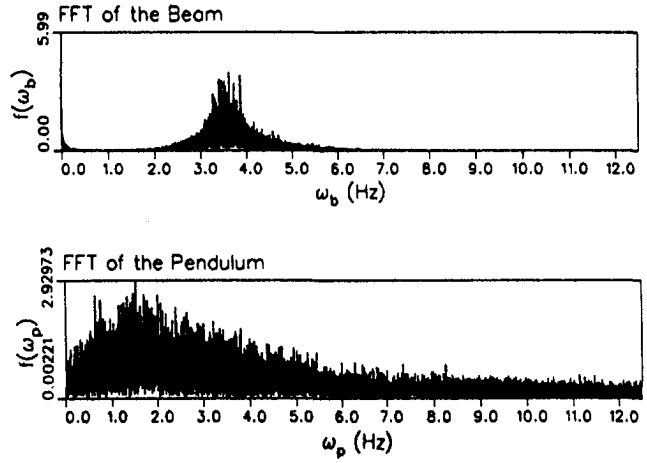

Fig. 11 FFT of the beam pendulum system for the forcing frequency of 3.50 Hz, f = 0.00175 m, and $m_p/m \approx 1/4$

$\omega_b = 2\omega_p = \Omega = 3.07$ Hz. However, as shown in Fig. 6, the beam energy is almost diminished and, consequently, its amplitude is collapsed when $\Omega = 3.10$ Hz. It is, of course, difficult to tune the pendulum precisely to the internal resonance condition of $\omega_b = 2\omega_p$ Hz and, as a result, instead of having the most energy absorption action at the exact internal resonance condition of $\omega_b = 2\omega_p = 3.07$ Hz, it takes place at $\Omega = 3.10$ Hz. It is interesting to note that the pendulum now has a nice periodic motion, as can be seen from Figs. 10(c), 10(d), and 10(f). Figure 10(b) shows that the coupling effect of the pendulum on the beam still exists, and one can assume that this is the dominant energy which oscillates the beam slightly about the static equilibrium position.

As shown in Fig. 7, after the critical region, the system reaches to second jump phenomenon at approximately $\Omega = 3.55$ Hz for both excitation amplitudes, $f = 0.00025\ m$ and $f = 0.00175\ m$. At this frequency, both the beam and the pendulum lose their stability and jump to another stable point. To reach the steady-state response at this point, the experiment is continued for approximately 3 minutes. The forcing frequency is then swept until $\Omega = 3.8$ Hz. When the forcing frequency is approximately between 3.48 Hz and 3.58 Hz, the system goes to chaotic motion. In other words, system response does not show any regular pattern even after a long time. Right after the chaotic motion, the system reaches the new steady-state motion at a forcing frequency $\Omega = 3.58$ Hz. Although the experiment was conducted for 2 hours and 25 minutes at a forcing frequency of 3.50 Hz, only 130,000 data points were recorded during the last 25 minutes. A short piece of the record is presented in Fig. 11. From Fig. 11, it is evident that the time histories are not regular and the FFT shows numerous peaks.

For the results of the experiment shown in Fig. 12, the mass ratio of the beam and the pendulum are taken to be approximately $\frac{1}{32}$. The natural frequency of the beam becomes $\omega_b = 3.38$ Hz, and the natural frequency of the pendulum is set to $\omega_p = 1.69$ Hz to maintain the condition of autoparametric interaction. Experiments are carried out with the same parameters as the previous ones. This figure illustrates that even the system is excited with low forcing amplitude, the system loses its periodicity within the autoparametric interaction region.

Furthermore, to investigate the unabsorbed motion of the beam, the mass of the pendulum (m_p = 54 gr) is combined with the tip mass of the beam (m = 212 gr) and experiments are performed with the tip mass (m = 266 gr) without the pendulum (Fig. 13). Thus the beam natural frequency, 3.07 Hz, remains the same as in the first experiment shown in Fig. 6. Comparison of Fig. 6 with Fig. 13 for the forcing amplitude of 0.00025 m, reveals that the deflection of the beam is considerably reduced. As shown in Fig. 6, the beam response is significantly diminished in the neighborhood of the natural frequency of the beam.

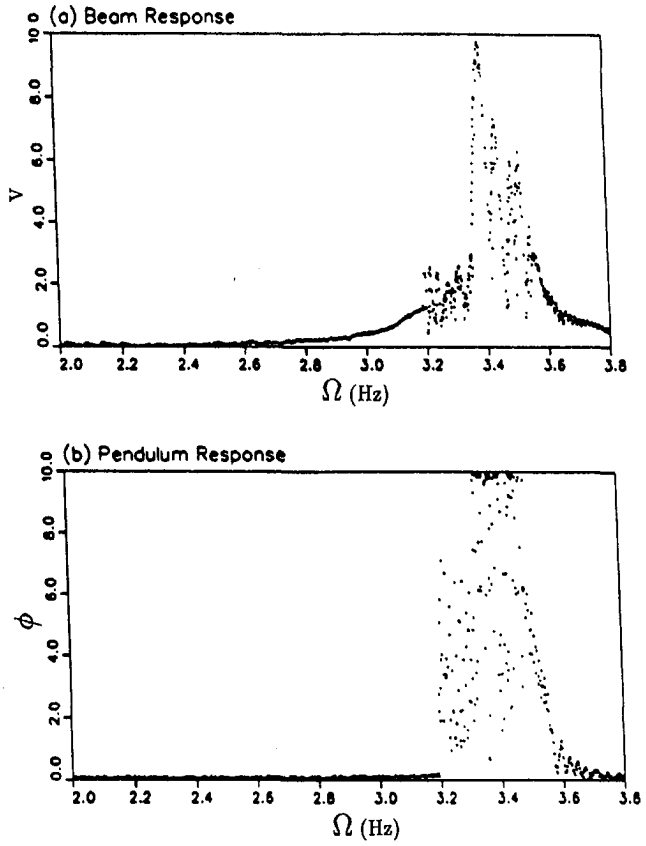

Fig. 12 Frequency response curves for f = 0.00175 m and $m_p/m \approx 1/32$

The theoretical results agree well with the experimental results quantitatively. Although experimental results show a stronger coupling effect as well as a higher energy exchange than those predicted theoretically, the energy exchange and, consequently, the absorption action through the pendulum is evident from both approaches (see Figs. 2 and 6). The quantitative discrepancy between the experiment and theoretical results is due to neglecting the effect of the higher modes in the theory when the Galerkin Method is used.

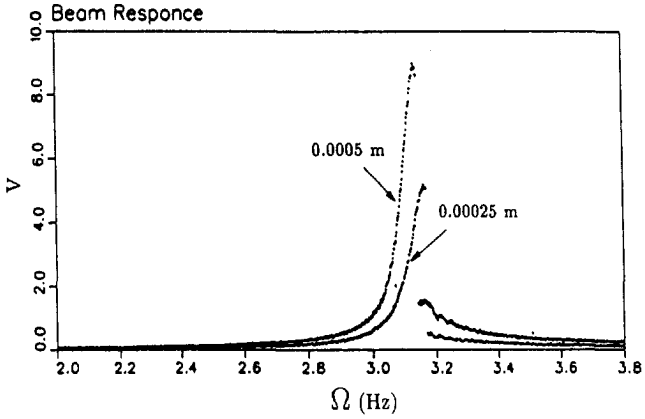

Fig. 13 Unabsorbed response of the beam for f = 0.00025 m, and f = 0.00050 m

Downloaded From: https://vibrationacoustics.asmedigitalcollection.asme.org on 07/02/2019 Terms of Use: http://www.asme.org/about-asme/terms-of-use

6 Conclusion

This paper presents the nonlinear equations of motion to investigate the autoparametric interaction between the first two modes of a beam-tip mass-pendulum system. Numerical integration is used to demonstrate some of the analytical results for various pendulum damping coefficients and beam pendulum mass ratios. The results showed that autoparametric interaction between the beam and the pendulum modes occurs when the external resonance condition of $\Omega = \omega_b$ and the primary resonance condition of $\omega_b = 2\omega_p$ are satisfied. Furthermore, experiments were performed to substantiate the energy transfer between the beam and pendulum predicted theoretically. Particularly, energy absorbtion by the pendulum in the neighborhood of the internal resonance conditions has been qualitatively verified. In conclusion, the results of this research validate the concept of using a pendulum as vibration absorber for flexible structures.

7 References

Arnold, F. R., 1955, "Steady-State Behavior of Systems Provided with Nonlinear Dynamic Vibration Absorbers," ASME *Journal of Applied Mechanics,* pp. 487–492.

Banerjee, B., Bajaj, K. A., and Davies, P., 1993, "Second Order Averaging Study of an Autoparametric System," 1993 ASME Design Technical Conferences-14th Biennial Conference on Mechanical Vibration and Noise, DE-Vol. 54, pp. 127–138.

Crossley, F. R. E., and Conn, N. H., 1953, "The Forced Oscillation of the Centrifugal Pendulum with Wide Angles," ASME *Journal of Applied Mechanics,* pp. 41–47.

Ertas, A., and Chew, E. K., 1990, "Nonlinear Dynamic Response of a Rotating Machine," *International Journal of Nonlinear Mechanics,* Vol. 25, pp. 241–251.

Ertas, A., and Mustafa, G., 1992, "Real-Time Response of the Simple Pendulum: An Experimental Technique," *Experimental Techniques,* Vol. 16, No. 4, pp. 33–35.

Eugene, S., 1961, "On the Parametric Excitation of Pendulum Type Vibration Absorber," ASME *Journal of Applied Mechanics,* pp. 330–334.

Gurgoze, M., 1986, "On the Approximate Determination of the Fundamental Frequency of a Restrained Cantilever Beam Carrying a Tip Heavy Body, *Journal of Sound and Vibration,* Vol. 105, No. 3, pp. 443–449.

Haddow, A. G., Barr, A. D. S., and Mook, D. T., 1984, "Theoretical and Experimental Study of Modal Interaction in a Two Degree of Freedom Structure," *J. Sound Vib.,* Vol. 97, No. 3, pp. 451–473.

Hatwal, H., 1982, "Notes on an Autoparametric Vibration Absorber," *Journal of Sound and Vibration,* Vol. 83, No. 3, pp. 440–443.

Hatwall, H., Mallik, A. K., and Ghosh, A., 1983a, "Forced Nonlinear Oscillations of an Autoparametric Systems—Part 1: Periodic Response," ASME *Journal of Applied Mechanics,* Vol. 50, pp. 657–662.

Hatwall, H., Mallik, A. K., and Ghosh, A., 1983b, "Forced Nonlinear Oscillations of an Autoparametric Systems—Part 2: Chaotic Response," ASME *Journal of Applied Mechanics,* Vol. 50, pp. 663–668.

Haxton, R. S., and Barr, A. D. S., 1972, "The Autoparametric Vibration Absorber," ASME *Journal of Engineering for Industry,* pp. 119–125.

Hunt, J. B., and Nissen, J-C., 1982, "The Broadband Dynamic Vibration Absorber," *J. Sound Vib.,* Vol. 83, No. 4, pp. 573–578.

Ibrahim, R. A., 1975, "Autoparametric Resonance in a Structure Containing Liquid—Part 1: Two mode Interaction," *J. Sound Vib.,* Vol. 42, No. 2, pp. 159–179.

Ibrahim, R. A., and Barr, A. D. S., 1978, "Parametric Vibration—Part 2: Mechanics of Nonlinear Problems," *Shock Vib. Digest,* Vol. 10, No. 2, pp. 41–57.

Kojima, H., Nagaya, K., Shiraishi, H., and Yamashita, A., 1985, "Nonlinear Vibration of a Beam with a Mass Subjected to Alternating Electromagnetic Force," *Bulletin of JSME,* Vol. 28, pp. 468–474.

Laura, P. A. A., Pombo, J. L., and Susemihl, E. A., 1974, "A Note on the Vibrations of a Clamped-Free Beam with a Mass at the Free End," *Journal of Sound and Vibration,* Vol. 37, No. 2, pp. 161–168.

Liu, W. H., and Huang, C. C., 1988, "Vibrations of a Constrained Beam Carrying a Heavy Tip Body," *Journal of Sound and Vibration,* Vol. 123, No. 1, pp. 15–29.

Ludeke, C. A., 1942, "Resonance," *Journal of Applied Physics,* Vol. 13, pp. 418–423.

Masri, S. F., and Caughey, T. K., 1966, "On the Stability of the Impact Damper," ASME *Journal of Applied Mechanics,* pp. 586–592.

Masri, S. F., 1972, "Theory of the Dynamic Vibration Neutralizer with Motion-Limiting Stops," ASME *Journal of Applied Mechanics,* pp. 563–568.

Nageswara Rao, B., Shastry, B. P., and Venkateswara Rao, G., 1986, "Large Deflections of a Cantilevered Beam Subjected to a Tip Concentrated Rotational Load," *Aeronautical Journal,* pp. 262–266.

Nissen, J.-C., Popp, K., and Schmalhorst, B., 1985, "Optimization of a Nonlinear Dynamic Vibration Absorber," *Journal of Sound and Vibration,* Vol. 99, No. 1, pp. 149–154.

Sato, K., Saito, H., and Otomi, K., 1978, "The Parametric Response of a Horizontal Beam Carrying a Concentrated Mass Under Gravity," ASME *Journal of Applied Mechanics,* Vol. 45, pp. 643–648.

Shaw, J., and Shaw, S. W., 1989, "The Onset of Chaos in a Two Degree of Freedom Impacting System," ASME *Journal of Applied Mechanics,* Vol. 56, pp. 168–174.

Struble, R. A., and Heinbockel, J. H., 1963, "Resonant Oscillation of a Beam-Pendulum System," ASME *Journal of Applied Mechanics,* pp. 181–188.

Storch, J., and Gates, S., 1985, "Transverse Vibration and Buckling of a Cantilever Beam with Tip Body Under Axial Acceleration," *Journal of Sound and Vibration,* Vol. 99, No. 1, pp. 43–52.

Szemplinska-Stupnica, W., 1969, "On the Phenomenon of the Combination Type Resonance in Nonlinear Two Degree of Freedom Systems," *Intl. J. Nonlinear Mech.,* Vol. 4, No. 4, pp. 336–359.

Tomas, J., 1967, "The Contribution to the Problem of Internal Resonance in a Nonlinear System with Two Degrees of Freedom," *Proc. 4th Conf. Nonlinear Oscill.,* Prague, pp. 503–508.

Tondl, A., 1963, "On the Combination Resonance of a Nonlinear Systems with Two Degrees of Freedom," *Rev. Mech. Appl.,* Vol. 8, No. 4, pp. 573–588.

Verma, M. K., and Murthy, A. V. Krishna, 1978, "Non-linear Vibration of Non-uniform Beams with Concentrated Masses," *Journal of Sound and Vibration,* Vol. 100, pp. 487–491.

Zavodney, L. D., and Nayfeh, A. H., 1989, "The Nonlinear Response of a Slender Beam Carrying a Lumped Mass to a Principal Parametric Excitation: Theory and Experiment," *Int. J. Non-Linear Mechanics,* Vol. 24, No. 2, pp. 105–125.

Downloaded From: https://vibrationacoustics.asmedigitalcollection.asme.org on 07/02/2019 Terms of Use: http://www.asme.org/about-asme/terms-of-use